Chinese Journal of Polymer Science Vol. 33, No. 11, (2015), 1550–1561

Chinese Journal of Polymer Science
© Chinese Chemical Society
Institute of Chemistry, CAS
Springer-Verlag Berlin Heidelberg 2015

The Effect of Particle Shape on the Structure and Rheological Properties of Carbon-based Particle Suspensions*

Ran Niu[a, b], Jiang Gong[a, b], Dong-hua Xu[a**], Tao Tang[a] and Zhao-yan Sun[a**]

[a] *State Key Laboratory of Polymer Physics and Chemistry, Changchun Institute of Applied Chemistry, Chinese Academy of Sciences, Changchun 130022, China*

[b] *University of Chinese Academy of Sciences, Beijing 100049, China*

Abstract The structure and rheological properties of carbon-based particle suspensions, *i.e.*, carbon black (CB), multi-wall carbon nanotube (MWNT), graphene and hollow carbon sphere (HCS) suspended in polydimethylsiloxane (PDMS), are investigated. In order to study the effect of particle shape on the structure and rheological properties of suspensions, the content of surface oxygen-containing functional groups of carbon-based particles is controlled to be similar. Original spherical-like CB (fractal filler), rod-like MWNT and sheet-like graphene form large agglomerates in PDMS, while spherical HCS particles disperse relatively well in PDMS. The dispersion state of carbon-based particles affects the critical concentration of forming a rheological percolation network. Under weak shear, negative normal stress differences (ΔN) are observed in CB, MWNT and graphene suspensions, while ΔN is nearly zero for HCS suspensions. It is concluded that the vorticity alignment of CB, MWNT and graphene agglomerates under shear results in the negative ΔN. However, no obvious structural change is observed in HCS suspension under weak shear, and accordingly, the ΔN is almost zero.

Keywords: Particle shape; Surface chemistry; Negative normal stress differences; Structure; Interaction.

Electronic Supplementary Material Supplementary material is available in the online version of this article at http://dx.doi.org/10.1007/s10118-015-1704-1.

INTRODUCTION

Incorporating inorganic particles is widely used as a low cost route to improve the properties of the suspended medium. Among these fillers, carbon-based particles including carbon black (CB), carbon nanotube, graphene, C_{60} and carbon sphere have attracted significant scientific and technological interest, due to their superior electrical, thermal and mechanical properties[1, 2].

The dispersion and structure of particle/polymer suspensions are closely related with their properties and final applications. Many factors can influence the dispersion of carbon-based particles, such as surface chemistry and aspect ratio of particles[3–7], molecular weight and viscosity of polymer matrix[8, 9], and so on. In previous work, the dispersion and structure of carbon-based particles in different polymers have been investigated[4–9]. However, the influence of particle shape and inter-particle interaction on the dispersion of carbon-based particles has not been systematically explored yet.

One of the hot topics of incorporating particles into polymers is the influence on the rheological properties

* This work was financially supported by the National Natural Science Foundation of China (Nos. 21474111, 21222407 and 21274152) and subsidized by the National Basic Research Program of China (973 Program, 2012CB821500).
** Corresponding authors: Dong-hua Xu (许东华), E-mail: dhxu@ciac.ac.cn
Zhao-yan Sun (孙昭艳), E-mail: zysun@ciac.ac.cn
Received April 9, 2015; Revised May 20, 2015; Accepted May 22, 2015
doi: 10.1007/s10118-015-1704-1

of composites, which is related with the processing and transport properties of the composites. Carbon-based particle suspensions exhibit rich rheological behaviors: shear banding[5, 10], viscosity reduction[11, 12], shear thickening[13] and negative normal stress differences[5, 9, 14, 15], *etc*. A surprising rheological property of carbon-based particle suspensions and composites is the negative normal stress differences (ΔN) observed under shear[5, 9, 14–17], which is rarely observed in other soft condensed matter. In our previous work, we observed negative ΔN in carbon black/silicone oil suspensions[16], MWNT/low molecular weight polydimethylsiloxane (PDMS, below the critical entanglement molecular weight M_c) suspensions[5] and graphene oxide/low molecular weight PDMS suspensions[9]. However, these carbon-based particles have different surface chemistry properties. When the surface chemistry properties of these carbon-based particles are similar, how particle shape and inter-particle interaction affect the structure and rheological properties of carbon-based particle suspensions has not been examined yet.

In this work, the surface chemistry of carbon-based particles, *i.e*., CB, MWNT, graphene and hollow carbon sphere (HCS), is controlled by the content of surface oxygen-containing functional groups. Low molecular weight (below M_c) polydimethylsiloxane (PDMS) is used as the matrix. The structure and rheological properties of these carbon-based particle suspensions are explored.

EXPERIMENTAL

Materials and Preparation of Samples

Carbon black (CB, purity > 99%) was purchased from Linzi Qishun Chemical Co., Shandong, China. To decrease the content of oxygen-containing functional groups, CB was pretreated with a mixture of N_2 and H_2 gas in a 9/1 volume ratio at 820 °C for 2 h in a fixed bed reactor. Multiwall carbon nanotubes (MWNTs, diameter 10–20 nm, length 10–30 μm) were prepared by chemical vapor deposition method and were kindly supplied by Timesnano (Chengdu Organic Chemicals Co. Ltd, Chinese Academy of Sciences). Graphene (code KNG-G5, thickness < 5 nm, size 0.1–5 μm, and purity > 99%) was obtained from Xiamen Knano Graphene Technology Co., Ltd., Xiamen, China. To increase the content of oxygen-containing functional groups, graphene was refluxed in concentrated HNO_3 solution (65 wt%) at 110 °C for 3 h. Hollow carbon sphere (HCS) with an average diameter of 91 nm as measured by image analysis (Fig. S1 in the supporting information (SI)) was prepared by catalytic carbonization of polystyrene[18]. Trimethyl-terminated PDMS with molecular weight (M_w) of 14000 g/mol and density of 0.97 g/cm^3 at 25 °C was supplied by Alfa Aesar.

Carbon-based particle suspensions were prepared by solution blending method. A designed amount of CB, graphene or HCS was dispersed in tetrahydrofuran (THF) (0.1 wt%) by sonication (150 W) for 1 h. MWNT was dispersed in THF (0.1 wt%) by sonication (150 W) for 5 min to avoid sonication induced shortening of MWNTs. PDMS was mixed with a certain volume of carbon-based particle/THF suspension to obtain desired concentration of carbon-based particles in PDMS. The resultant mixtures were mechanically stirred for 1 h and then poured into Petri dish to dry. Finally, samples were further dried in a vacuum oven at 25 °C for 18 h to remove residual solvent.

Characterization

Transmission electron microscopy (TEM, JEM-1011) was used to observe the morphology of carbon-based particles at an accelerating voltage of 100 kV. X-ray photoelectron spectroscopy (XPS) was used to characterize the surface element composition of carbon-based particles on a VG ESCALAB MK II spectrometer using an Al Kα exciting radiation from an X-ray source operated at 10.0 kV and 10 mA. The textural property of carbon-based particles was measured by N_2 sorption at 77 K using a Quantachrome Autosorb-1C-MS analyzer. The specific surface area was calculated by BET method. Wide-angle X-ray diffraction (WAXD) was employed to measure the interlayer spacing of graphene powder and graphene in suspensions with a Rigaku model D max 2500 with a Cu Kα radiation.

Small-angle X-ray scattering (SAXS) experiments were carried out with the aid of a semiconductor detector (Pilatus 100K, DECTRIS, Swiss) attached to a conventional Ni-filtered Cu Kα X-ray source (GeniX3D Cu

ULD, Xencos SA, France). The wavelength of the X-ray radiation is 0.154 nm. The sample-to-detector distance is 6000 mm, where the effective range of the scattering vector q ($q = 4\pi/\lambda\sin\theta$, where 2θ is the scattering angle and λ is the wavelength) is 0.2–2 nm^{-1}. Each SAXS pattern obtained in the center of the sample was collected within 60 min; background was corrected and normalized using the standard procedure.

The dispersion state of carbon-based particles in PDMS was observed with an Olympus BX-51 optical microscope under bright field. Optical observations under shear were carried out using a Linkam CSS-450 shearing cell equipped with an optical microscope. Optical micrographs were taken in the x-z plane with flow along the x axis, a constant velocity gradient along the y axis, and vorticity along the z axis. Samples were confined between two parallel quartz plates separated by a fixed gap (100 μm). The lower plate rotates at an angular speed that sets the shear rate, $\dot{\gamma} = \partial v_x/\partial y$, and a fixed point is used for observation. The samples were sheared at constant shear rates for 2 min to explore the structural change under shear. All the optical observations were carried out at 25 °C.

Rheological measurements were performed on an ARES G2 instrument (TA Instruments, strain controlled rheometer) with 25 or 50 mm parallel-plate geometry. After the sample was loaded on the geometry, the sample was squeezed with an axial force lower than 0.05 N. Before the measurements, the sample was left at rest for at least 10 min to wait for the decay of axial force (~10^{-3} N). Oscillatory strain sweep experiments were conducted at a frequency of 1 rad/s to determine the linear viscoelastic region. Linear oscillatory frequency sweeps were performed from 0.05 rad/s to 100 rad/s at appropriate strain in the linear region. Steady shear experiments were carried out from 0.01 s^{-1} to 100 s^{-1}. Start-up shear experiments were performed at different shear rates from rest. For parallel-plate geometry, the measured normal stress is actually a difference of the normal stress differences, $\Delta N \equiv N_1 - N_2$ (the normal stress differences N_1 and N_2 are defined as ($\tau_{11} - \tau_{22}$) and ($\tau_{22} - \tau_{33}$), respectively, where τ_{ii} represent the normal stresses acting along the flow (1), flow gradient (2) and vorticity (3) directions)[19]. All the experiments were performed at 25 °C.

RESULTS AND DISCUSSION

Morphology of Original Carbon-based Particles

Transmission electron microscopy (TEM)

The morphology of carbon-based particles was observed by TEM. In Fig. 1(a), multi-armed CB agglomerates are observed. This multi-armed structure of CB is formed by aggregates as a result of the van der Waals interaction. On a smaller scale, spherical-like CB aggregates (~50 nm) are observed[20, 21], which was reported to be fused by several smaller spherical primary carbon particles (~10 nm)[21–23]. In Figs. 1(b) and 1(c), the morphologies of rod-like MWNT and sheet-like graphene are shown, respectively. In Fig. 1(d), big HCS agglomerates are also observed, which are formed during the evaporation of solvent on cupper grid.

X-ray photoelectron spectroscopy (XPS)

The surface chemistry property of carbon-based particles was analyzed by XPS. As shown in Fig. 2, the surface oxygen content of carbon-based particles is similar, with an average value of 9.3%. The peaks in the C1s spectra of carbon-based particles (Fig. S2) indicate that carbon atoms are in four different functional groups: the non-oxygenated ring C (284.8 eV), the C in C—O bond (286.2 eV), the carbonyl C (C=O, 287.8 eV) and the carboxylate C (O—C=O, 289.0 eV)[24]. The oxygen atom on carbon-based particles originates from carbonyl, carboxyl and hydroxyl groups[9]. It is seen that there is hydrogen-bonding interaction between carbon-based particles. Moreover, the strength of hydrogen bonding interaction between carbon-based particles is expected to be close as the content of oxygen atom on the surface of carbon-based particles shows no obvious differences.

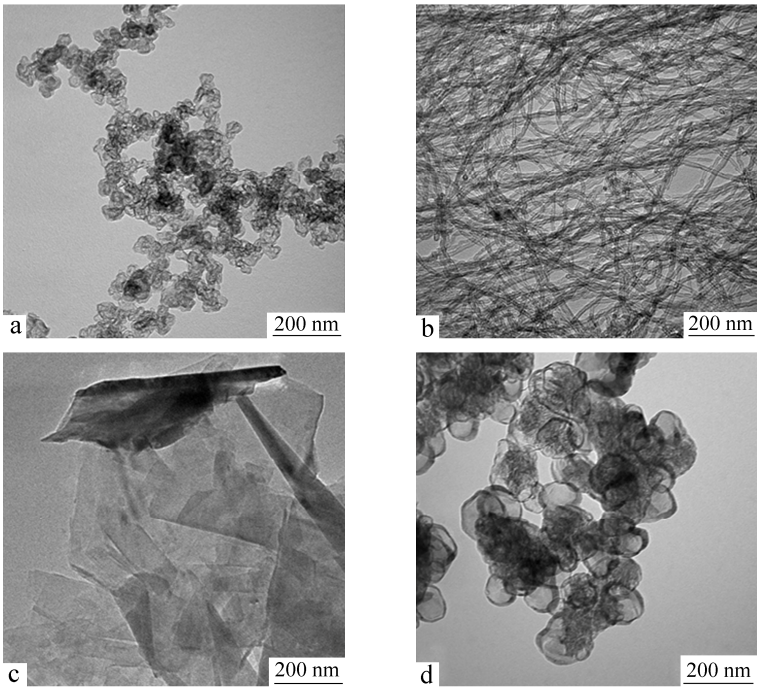


Fig. 1 TEM images of CB (a), MWNT (b), graphene (c) and HCS (d)

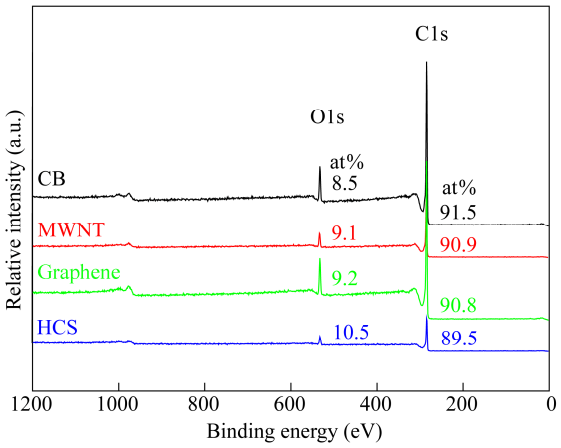


Fig. 2 Overall XPS spectra of carbon-based particles

Structure of Carbon-based Particle Suspensions

Wide-angle X-ray diffraction (WAXD)

WAXD was used to detect the interlayer spacing of graphene and the exfoliation extent of graphene in PDMS. The WAXD patterns of graphene powder, PDMS and 14 wt% graphene/PDMS suspension are displayed in Fig. 3. A sharp diffraction peak at $2\theta = 26.7°$ originates from the interlayer (002) spacing ($d = 0.34$ nm) of graphite[25]. For PDMS, there is a broad and weak diffraction peak at 12.5°[26]. When dispersed in PDMS, the sharp diffraction peak of graphene weakens, indicating that graphene is partially exfoliated. The weak diffraction peak for graphene/PDMS at $2\theta = 26.9°$ indicates that some graphene platelets with smaller interlayer spacing remain un-dispersed in PDMS.

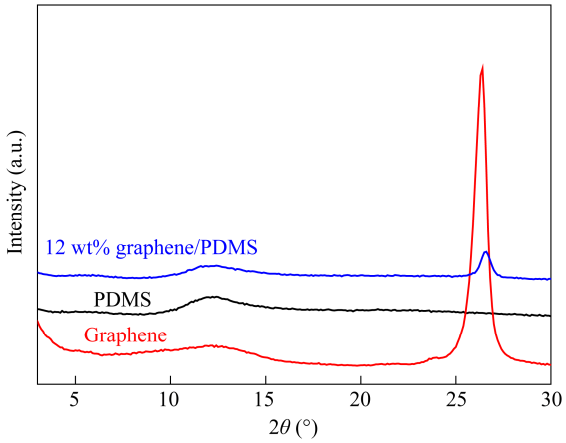


Fig. 3 WAXD patterns of graphene powder, PDMS and 14 wt% graphene/PDMS suspension (Intensity profiles are vertically shifted for clarity.)

Small angle X-ray scattering (SAXS)

SAXS measurements were performed to investigate the structure of carbon-based particles in PDMS on the length scale of 3–31 nm, evaluated as $d = 2\pi/q$ where d is the length of scattering objects and q is the scattering vector[27]. The scattering curves are analyzed using Beaucage's Unified Model[28] to extract relevant length scales and exponents.

Figure 4 and Fig. S3 show the log-log plot of intensity profiles of carbon-based particle suspensions with low and high particle concentrations. It is demonstrated that the scattering curves of CB, MWNT and HCS suspensions exhibit crossover feature. The two crossovers for CB suspension at $q^* = 0.35$ and 1.24 nm^{-1} are associated with the size of primary carbon particles (17.9 nm) constituting CB aggregates and the stacking of graphitic layers (5.6 nm). In the low q range ($d > 17.9$ nm), the slope of –2.98 for CB suspension indicates the mass fractal of CB aggregates with fractal dimension of 2.98 (close to 3, scattering of spherical structure)[21], which is consistent with the spherical-like structure of CB aggregates in Fig. 1(a). In the intermediate q range (5.6 nm < d < 17.9 nm), the slope of –3.24 reflects the highly rough and surface fractal structure of primary carbon particles with fractal dimension of 2.76 (Fig. 1a)[23]. In the high q range ($d < 5.6$ nm), the deviation from q^{-2} (scattering of plate-like structure) may be a result of the turbostratic structure of graphitic layers[21, 29].

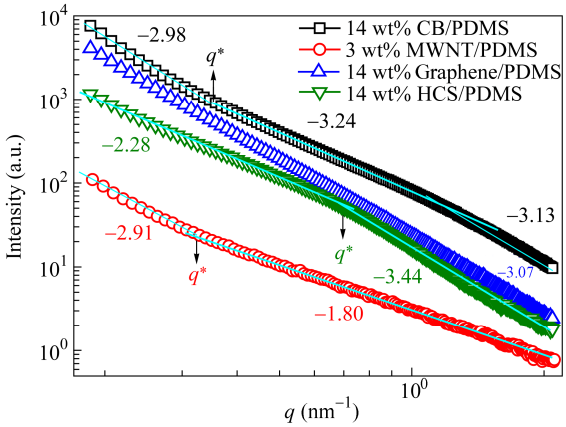


Fig. 4 SAXS profiles of carbon-based particle suspensions with high particle concentrations

For MWNT/PDMS suspension, the crossover at $q^* = 0.45$ nm^{-1} is associated with the diameter of MWNT (13.9 nm). In low q range ($d > 13.9$ nm), the slope of –2.91 for MWNT suspension strongly indicates the

aggregation[30, 31], as power law between –2 and –3 is possible for objects such as a large flat disk or a disk with a convoluted surface.

For HCS suspension, the crossover at $q^* = 0.70$ nm^{-1} corresponds to the thickness of HCS shell (9.0 nm). In low q range ($d > 9.0$ nm), the slope of –2.28 for HCS suspension indicates the aggregation of HCS[30, 31]. In high q range ($d < 9.0$ nm), the slope of –3.44 suggests the highly rough surface of HCS[23].

For graphene/PDMS suspensions, $I(q)$ scales with $q^{-3.07}$ in the investigated q range, indicating the surface fractal of graphene sheets with fractal dimension of 2.93[32], which is in a good agreement with the crumpled surface of graphene (Fig. 1c).

The concentration of carbon-based particles has little influence on the structure of carbon-based particle suspensions (Fig. S3), which is consistent with Rahatekar's results[33].

Optical Microscope

The structure of carbon-based particles in PDMS was further explored by optical microscope on the length scale of micrometer. As shown in Fig. 5, there are some agglomerates in carbon-based particle suspensions and the size of agglomerates was measured by plotting a circle around each agglomerates. The average sizes of the agglomerates for 0.5 wt% CB/PDMS, MWNT/PDMS and graphene/PDMS suspensions are 26.3, 60.0 and 11.3 μm, respectively. In Koga's work about the structure of CB in polymer matrix, CB agglomerates (~20 μm) were determined to have mass-fractal structure (multi-armed structure)[23], which may be consistent with the structure of CB agglomerates in this work. In Fig. 5(d), HCS particles disperse relatively well in PDMS as only a small portion of smaller agglomerates with an average size of 4.2 μm are observed.

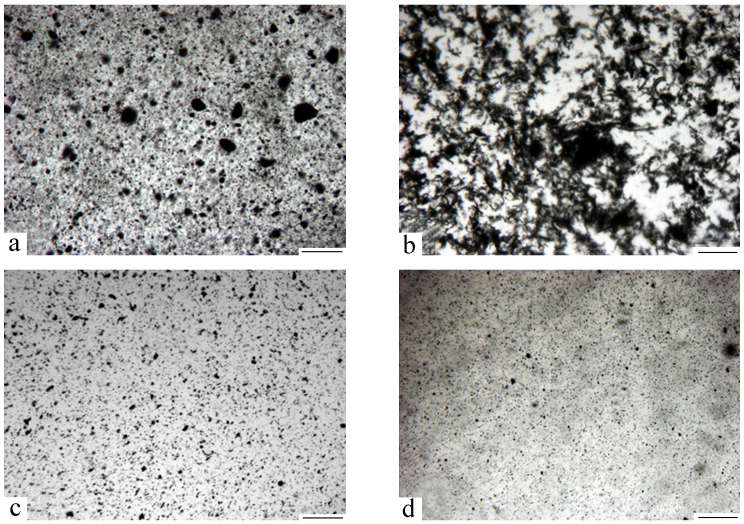


Fig. 5 Optical micrographs of 0.5 wt% CB/PDMS (a), 0.5 wt% MWNT/PDMS (b), 0.5 wt% graphene/PDMS (c) and 0.5 wt% HCS/PDMS suspensions (d) (The scale bars are 150 μm.)

The inter-particle interaction and polymer-particle interaction determine the dispersion state of carbon-based particles. The attractive interaction between carbon-based particles, such as π-π interaction[34] and hydrogen-bonding interaction, is partially responsible for the aggregation. CB particle has lower graphitization degree, thus the inter-particle π-π attractive interaction should be weaker[18, 35]. However, due to the large specific surface area, CB (1369.4 m^2/g) is more prone to aggregate than the other carbon-based particles (see Table S1 in SI)[36]. HCS particle also has lower graphitization degree and the inter-particle π-π interaction should be weaker[8, 35]. Moreover, according to the Hamaker or Lifshitz theory, the van der Waals interaction between particles depends on the geometry of the particle and the dielectric permittivities of various materials concerned[37, 38]. Thus the air or PDMS in the hollow carbon sphere and the shape of sphere would make the van der Waals interaction between HCS weaker than that of the other carbon-based particles[37, 38]. Accordingly, the

size and fraction of HCS agglomerates are smaller than those of the other agglomerates. For MWNT and graphene, the inter-particle π-π attractive interaction should be larger than that of CB and HCS, which can induce the aggregation of MWNT and graphene. Moreover, MWNT with high aspect ratio is easily entangled, which is another important factor inducing the aggregation of MWNTs[39]. Besides the inter-particle interactions, there is CH-π interaction between carbon-based particles and PDMS[34, 40, 41]. The apparent aggregation of CB, MWNT and graphene in PDMS indicates that the inter-particle interaction is larger than polymer-particle interaction. The relatively good dispersion of HCS in PDMS indicates that polymer-particle interaction is close to inter-particle interaction between HCS.

Critical Concentration for the Formation of Network in Carbon-based Particle Suspensions

Adding filler has obvious influence on the viscoelasticity of polymers[14, 16, 19, 33]. Above a critical concentration (c_{cr}), percolated network forms and the mechanical properties of the composites are changed. The c_{cr} of carbon-based particle suspensions is determined by linear rheological measurements[5–10]. In Fig. 6, for 6 wt% CB/PDMS suspension, the values of G' and G'' are small and close to the resolution limit of the rheometer, implying that no apparent network structure is formed[42]. When the concentration of CB is increased to 8 wt%, the storage modulus (G') is larger than loss modulus (G'') in the experimental frequency range, indicating the formation of a network structure[42]. Accordingly, the c_{cr} of CB/PDMS suspension is in the range of 6 wt%–8 wt%. As the concentration of CB is increased, G' increases and the frequency dependence of G' decreases, implying the formation of enhanced network structure. The c_{cr} of MWNT, graphene and HCS suspensions are determined by similar method (Figs. S4–S6) and the results are summarized in Table 1.

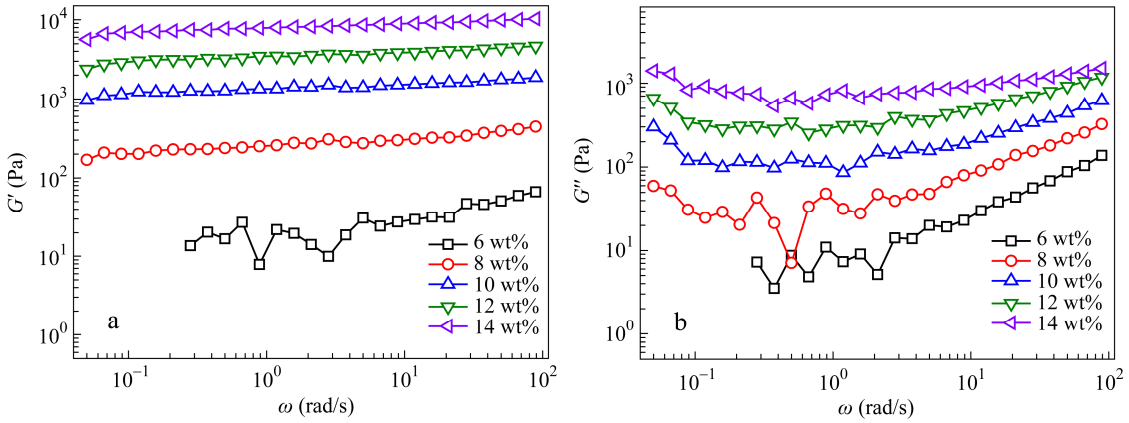


Fig. 6 Storage (G') and loss moduli (G'') versus frequency (ω) for CB/PDMS suspensions with different concentrations of CB

Table 1. Critical concentration (c_{cr} and m_c) for carbon-based particle/PDMS suspensions to form network

Samples	c_{cr} [a] (wt%)	m_c [b] (wt%)	R [c]
CB/PDMS	6.0–8.0	6.0	0.998
MWNT/PDMS	0.1–0.5	0.3	0.999
Graphene/PDMS	6.0–8.0	8.0	0.999
HCS/PDMS	12.0–14.0	13.9	0.997

[a] Estimated from the curve of G' and G'' versus frequency; [b] Obtained from power-law scaling of $G_0 \propto (m–m_c)^{\alpha}$; [c] Correlation coefficient for the linear fitting of $\lg G_0$ versus $\lg(m–m_c)$

For a more quantitative analysis, percolation scaling law is used to further determine the rheological percolation thresholds of carbon-based particle suspensions[43–45]. Above percolation threshold, the plateau modulus grows with the concentration of filler according to $G_0 \propto (m–m_c)^{\alpha}$[43–45], where G_0 is the plateau modulus obtained at small frequency (~0.12 rad/s), m is the mass fraction of filler, m_c is the rheological percolation threshold and α is the critical exponent. The details of fitting are shown in Figs. S7–S10 of SI, with correlation

coefficients above 0.997. The fitted results are shown in Table 1, which are consistent with the c_{cr} estimated directly from the curves of G' and G'' versus frequency.

Combined with the optical micrographs (Figs. 5a–5c), it is apparent that the networks of CB, MWNT and graphene suspensions are formed by the agglomerates[46, 47]. Moreover, MWNT suspension has the largest sized agglomerates and the lowest c_{cr}. The high aspect ratio of MWNT may also contribute to the lowest c_{cr}. It is well known that mono-disperse hard spheres can jam to form a stress-bearing network at random close packing with volume fraction of ~0.64[48]. The volume fraction at the c_{cr} of HCS suspensions is about 0.10 (the detailed calculation method is shown in the SI), indicating that the HCS network is also formed by the HCS agglomerates rather than by individual particles. And the smallest HCS agglomerates induce the highest c_{cr} of HCS suspensions.

Nonlinear Rheological Properties of Carbon-based Particle Suspensions

The flow behaviors of carbon-based particle suspensions give the basic knowledge for manufacturing process in industry, hence steady shear experiments were performed. As shown in Figs. 7(a) and 7(c), for CB and graphene suspensions with low particle concentrations, shear thinning is observed in the experimental shear rate range. As the concentration of CB or graphene is increased, three-region flow curves are observed, where shear thinning regions at low and high shear rates are separated by an intermediate plateau region. For MWNT suspensions (Fig. 7b), three-region flow curves are observed in the experimental concentration range, while simple shear thinning is found in HCS suspensions (Fig. 7d). At high shear rates, the surface fracture of 14 wt% CB/PDMS,

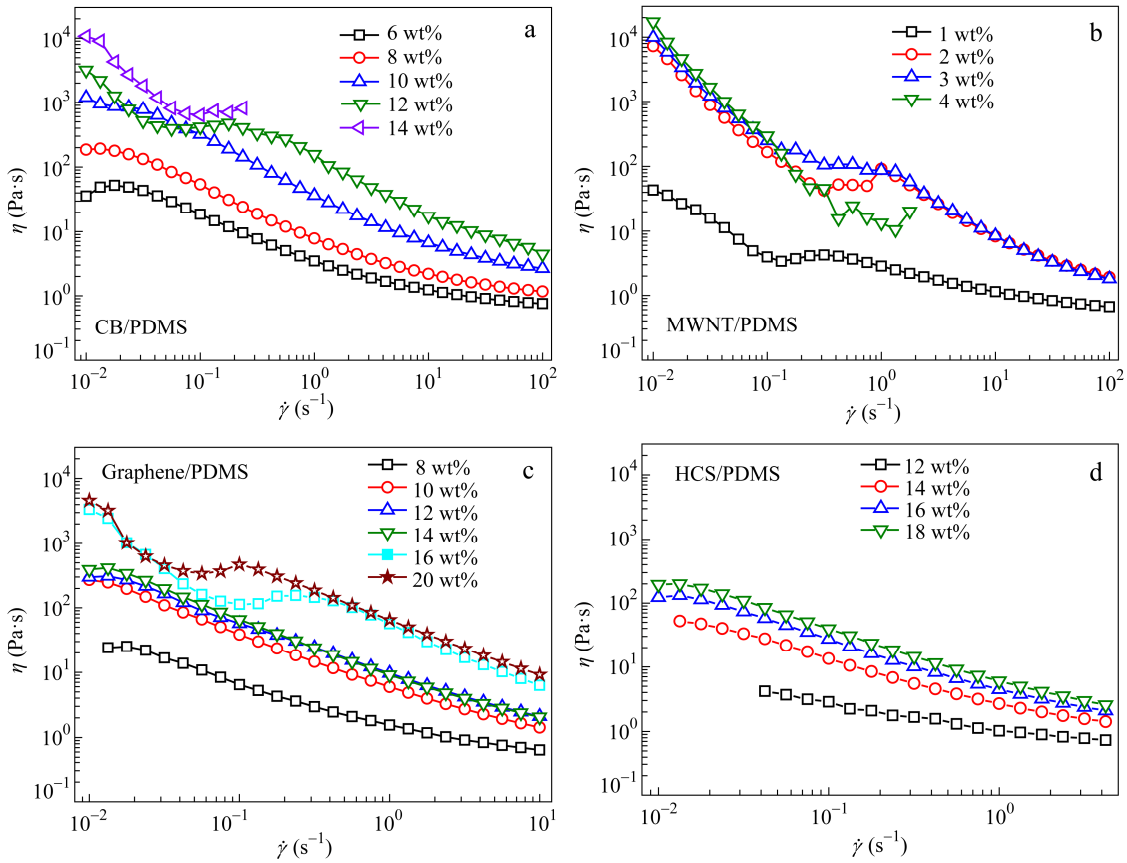


Fig. 7 Viscosity (η) as a function of shear rate ($\dot{\gamma}$) for CB/PDMS (a), MWNT/PDMS (b), graphene/PDMS (c) and HCS/PDMS suspensions (d)

4 wt% MWNT/PDMS and HCS/PDMS suspensions at the edge of geometry was observed, so these data are not shown in Fig. 7. The low-shear-rate viscosity of samples with the same concentration of particles (*e.g.*, 12 wt%) decreases as the agglomerate size of carbon-based particles decreases. The low-shear-rate viscosity of MWNT suspensions is higher than that of other samples with slightly higher concentration of particles, consistent with simulation result[49]. Thus larger sized agglomerates not only induce lower concentration to form a network structure but also stronger reinforcement effect of the suspended polymer.

In previous work, shear thinning and viscosity plateau were proposed to be caused by high yield stress which masks the shear thickening[50–52]. In this work, the slopes of η versus $\dot{\gamma}$ in the low shear thinning region for concentrated CB, MWNT and graphene suspensions are more negative than 1 (Fig. S11 in SI), which are related with the breakup of the formed agglomerates[5]. The detailed explanations for the shear thinning of carbon-based particle suspensions are shown in the following part. In this work, the viscosity plateau may be related with the yielding of large agglomerates.

Another interesting phenomenon observed in some carbon-based particle suspensions is the negative normal stress differences (ΔN). In Fig. 8 and Fig. S12, obvious negative ΔN is observed in CB, MWNT and graphene suspensions at low and intermediate shear rate ranges where viscosity plateau is observed. Moreover, the absolute value of ΔN increases as particle concentration is increased. Comparatively, the ΔN for HCS suspensions is nearly zero, which is close to the resolution limit of normal force transducer. The mechanism for the negative ΔN in carbon-based particle suspensions is explained in the later part.

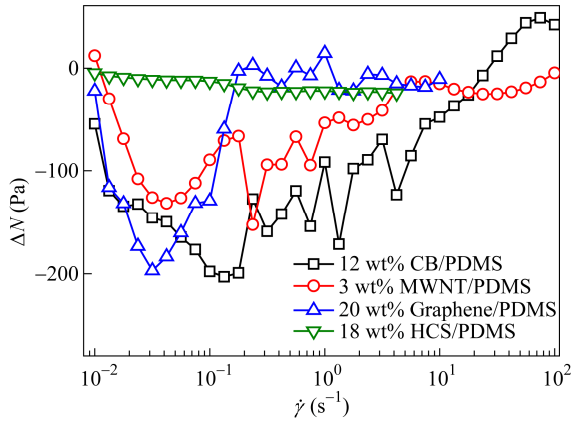


Fig. 8 Normal stress differences (ΔN) as a function of shear rate ($\dot{\gamma}$) for carbon-based particle suspensions

The transient shear behaviors of carbon-based particle suspensions at different shear rates are also explored and the results are shown in Fig. S13. Generally, negative ΔN is observed in CB, graphene and MWNT suspensions under weak shear ($\dot{\gamma} \leq 2$ s^{-1}), and zero ΔN is found in HCS suspensions, which are consistent with steady shear results. Moreover, the value of negative ΔN fluctuates as a result of the change of structure for anisotropic carbon-based particle suspensions[5]. Furthermore, the evolution of viscosity with time for above samples at different shear rates is shown in Fig. S14 in SI, which confirms that no edge fracture or lose of sample happened in the experimental time range.

Structural Change under Shear

In order to explore the microstructures of carbon-based particle suspensions under shear, *in situ* optical observation was performed. Imaging the structure of carbon-based particle suspensions at high concentrations is difficult due to the strong optical absorption, thus micrographs are taken at low particle concentrations. In Fig. 9, the agglomerates of CB roll up into short and isolated vorticity bands (see enlarged micrograph in Fig. S15 in SI) under weak shear ($\dot{\gamma} \leq 0.5$ s^{-1}). These vorticity aligned bands partially breakup and reform under weak shear (Fig. S16 in SI), leading to the fluctuation of negative ΔN (Fig. 9a)[5]. At high shear rates ($\dot{\gamma} = 2$ s^{-1}), the

agglomerates are broken into smaller ones or individual particles and align along the shear direction. For graphene/PDMS suspensions, the original agglomerates also roll up forming short isolated bands (Fig. S17 in SI) under weak shear ($\dot{\gamma} < 2$ s^{-1}), which have some degree of vorticity alignment similar to CB suspension.

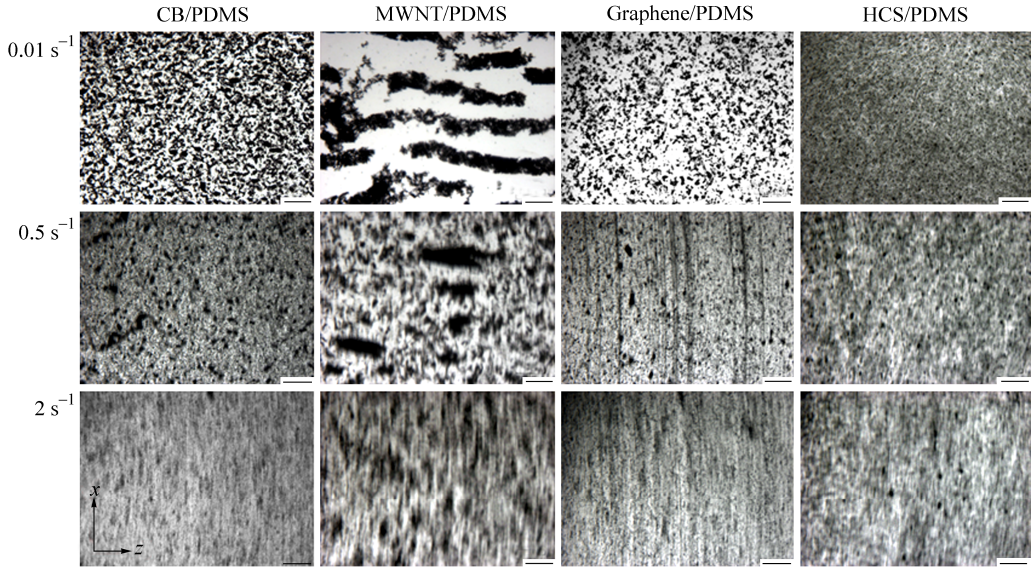


Fig. 9 Structures of 2 wt% CB/PDMS (a), 0.5 wt% MWNT/PDMS (b), 2 wt% graphene/PDMS (c) and 0.5 wt% HCS/PDMS suspensions (d) under different shear rates
The gap is 100 μm and scale bars are 150 μm. Photos are taken after shearing for ~30 s.

More obvious and longer vorticity bands are observed in MWNT/PDMS suspensions under weak shear ($\dot{\gamma}$ = 0.01 and 0.05 s^{-1}) compared with CB and graphene suspensions. These vorticity bands gradually break up when the shear rate is increased and completely disappear at $\dot{\gamma} = 2$ s^{-1}. However, no obvious structural change is observed in HCS/PDMS suspensions under weak shear, and HCS particles align along the shear direction at intermediate and high shear rates ($\dot{\gamma} \geq 2$ s^{-1}).

Correlated with steady shear results, the de-aggregation and alignment behaviors of big agglomerates induce the strong shear thinning of CB, MWNT and graphene suspensions (Fig. 7)[53]. Comparatively, weak shear thinning in HCS suspensions results from the rearrangement of small agglomerates to flow with less resistance[50].

The general nature of the fluid is also characterized to determine which factor induces the different shear behaviors of carbon-based particle suspensions. The Péclet number (*Pe*, ratio of shear rate to the rate of particle reorientation by Brownian motion) for carbon-based particle suspensions is calculated. The detailed calculation is shown in SI, and the calculated results are shown in Table S2. The calculated *Pe* for CB, MWNT and graphene suspensions are much larger than 1, indicating that Brownian motion of these particles can be neglected[19]. Thus weak shear induces the aggregation and vorticity alignment of CB, MWNT and graphene aggregates, which results in the negative ΔN[5, 15]. It should be noted that for MWNT/high molecular weight *i*PP composites, the sign of normal stress difference is positive[54, 55]. The difference results from the molecular weight of polymer matrix, as high molecular weight polymer (larger than M_c) restricts the vorticity alignment of MWNT aggregates and nonlinear stretching of entangled polymer chain partially induces positive ΔN[5, 55, 56]. Furthermore, network deformation may be not the main mechanism for the negative ΔN here, due to the low aspect ratio of CB or lower deformability of graphene[5].

However, the *Pe* for HCS suspension at low shear rates ($\dot{\gamma} < 1$ s^{-1}) is less than 1, suggesting that the shear force has little effect on the motion of HCS[19]. Hence, no shear induced aggregation or vorticity alignment is observed in HCS suspensions. At higher shear rates, the motion of HCS is controlled by shear force (*Pe* > 1) and

HCS particles align along the shear direction. Moreover, the PDMS matrix used in this work has almost zero ΔN (Fig. S18), thus the ΔN of HCS/PDMS suspensions is close to zero.

SUMMARY

The structure and rheological properties of carbon-based particle suspensions are investigated. In particular, the influence of original particle shape on the structure and rheological properties of carbon-based particle suspensions is examined. The differences in original particle shape and inter-particle interaction induce the different dispersion states of carbon-based particles, as indicated by the results of SAXS and optical microscope. Apparent agglomerates are observed in CB, MWNT and graphene suspensions, while HCS disperses relatively well in PDMS. It is concluded that the rheological percolation networks of these carbon-based particles are formed by the aggregation of agglomerates of original particles.

More interestingly, negative normal stress differences (ΔN) are observed in CB, MWNT and graphene suspensions with high particle concentrations. Correlated with optical-shear experiments, negative ΔN is inferred to be caused by the vorticity alignment of CB, MWNT and graphene agglomerates. Comparatively, nearly zero ΔN is found in Brownian HCS suspensions, as no obvious structural change is observed in HCS suspensions and the ΔN of pure PDMS is nearly zero in the experimental shear rate range. We expect this work will provide some guidance for the manufacturing and designing of carbon-based particle suspensions and composites.

REFERENCES

1 Baughman, R.H., Zakhidov, A.A. and de Heer, W.A., Science, 2002, 297: 787
2 Harris, P.J.F., Int. Mater. Rev., 2004, 49: 31
3 Kim, H., Miura, Y. and Macosko, C.W., Chem. Mater., 2010, 22: 3441
4 Lee, S.H., Cho, E., Jeon, S.H. and Youn, J.R., Carbon, 2007, 45: 2810
5 Niu, R., Gong, J., Xu, D.H., Tang, T. and Sun, Z.Y., RSC Adv., 2014, 4: 62759
6 Wu, D., Wu, L., Zhou, W.D., Sun, Y.R. and Zhang, M., J. Polym. Sci., Part B: Polym. Phys., 2010, 48: 479
7 Ye, L., Xie, Y., Qiu, D., Kan, Y. and Zhang, Z.D., Chinese J. Polym. Sci., 2014, 32(11): 1515
8 Kasaliwal, G.R., Göldel, A., Pötschke, P. and Heinrich, G., Polymer, 2011, 52: 1027
9 Niu, R., Gong, J., Xu, D.H., Tang, T. and Sun, Z.Y., Polymer, 2014, 55: 5445
10 Hobbie, E.K. and Fry, D.J., Phys. Rev. Lett., 2006, 97: 036101
11 Tan, H.Y., Xu, D.H., Wan, D., Wang, Y., Wang, L., Zheng, J., Liu, F., Ma, L. and Tang, T., Soft Matter, 2013, 9: 6282
12 Tan, Y.Q., Song, Y.H. and Zheng, Q., Nanoscale, 2012, 4: 6997
13 Sha, X.F., Yu, K.J., Cao, H.J. and Qian, K., J. Nanopart. Res., 2013, 15: 1816
14 Jun, S.I. and Lee, H.S., Appl. Phys. Lett., 2012, 100: 164108
15 Lin-Gibson, S., Pathak, J.A., Grulke, E.A., Wang, H. and Hobbie, E.K., Phys. Rev. Lett., 2004, 92: 048302
16 Niu, R., Gong, J., Xu, D.H., Tang, T. and Sun, Z.Y., Colloid Surface A, 2014, 444: 120
17 Osujia, C.O. and Weitz, D.A., Soft Matter, 2008, 4: 1388
18 Gong, J., Liu, J., Chen, X.C., Wen, X., Jiang, Z.W., Mijowska, E., Wang, Y.H. and Tang, T., Micropor. Mesopor. Mater., 2013, 176: 31
19 Kharchenko, S.B., Douglas, J.F., Obrzut, J., Grulke, E.A. and Migler, K.B., Nat. Mater., 2004, 3: 564
20 Rieker, T.P., Hindermann-Bischoff, M. and Ehrburger-Dolle, F., Langmuir, 2000, 16: 5588
21 Keefer, K.D. and Schaefer, D.W., Phys. Rev. Lett., 1986, 56: 2376
22 Koga, T., Takenaka, M., Aizawa, K., Nakamura, M. and Hashimoto, T., Langmuir, 2005, 21: 11409
23 Koga, T., Hashimoto, T., Takenaka, M., Aizawa, K., Amino, N., Nakamura, M., Yamaguchi, D. and Koizumi, S., Macromolecules, 2008, 41: 453

24 Briggs, D. and Beamson, G., "High resolution XPS of organic polymers: The Scienta ESCA300 Database" John Wiley & Sons Inc, New York, 1992
25 Szabó, T., Berkesi, O., Forgó, P., Josepovits, K., Sanakis, Y., Petridis, D. and Dékány, I., Chem. Mater., 2006, 18: 2740
26 Hernandez, R., Weksler, J., Padsalgikar, A. and Runt, J., Macromolecules, 2007, 40: 5441
27 Faiella, G., Piscitelli, F., Lavorgna, M., Antonucci, V. and Giordano, M., Appl. Phys. Lett., 2009, 95: 153106
28 Schaefer, D.W. and Keefer, K.D., Phys. Rev. Lett., 1986, 19: 2199
29 Jawhari, T., Roid, A. and Casado, J., Carbon, 1995, 33: 1561
30 Sun, C.H., Li, F., Ying, Z., Liu, C. and Cheng, H.M., Phys. Rev. B, 2004, 69: 033404
31 Saunders, J.M., Goodwin, J.W., Richardson, R.M. and Vincent, B., J. Phys. Chem. B, 1999, 103: 9211
32 Baskaran, D., Mays, J.W. and Bratcher, M.S., Chem. Mater., 2005, 17: 3389
33 Rahatekar, S.S., Koziol, K.K., Kline, S.R., Hobbie, E.K., Gilman, J.W. and Windle, A.H., Adv. Mater., 2009, 21: 874
34 Szabó, T., Berkesi, O., Forgó, P., Josepovits, K., Sanakis, Y., Petridis, D. and Dékány, I., Chem. Mater., 2006, 18: 2740
35 Donnet, J.B. and Vidal, A., Adv. Polym. Sci., 1986, 76: 103
36 Li, Y., Kröger, M. and Liu, K.W., Macromolecules, 2012, 45: 2099
37 Hobbie, E.K., Ihle, T., Harris, J.M. and Semler, M.R., Phys. Rev. B, 2012, 85: 245439
38 Smith, E.R., Mitchell, D.J. and Ninham, B.W., J. Colloid Interf. Sci., 1973, 45: 55
39 Hough, L.A., Islam, M.F., Janmey, P.A. and Yodh, A.G., Phys. Rev. Lett., 2004, 93: 168102
40 Beigbeder, A., Linares, M., Devalckenaere, M., Degée, P., Claes, M., Beljonne, D., Lazzaroni, R. and Dubois, P., Adv. Mater., 2008, 20: 1003
41 Suezawa, H., Yoshida, T., Ishihara, S., Umezawa, Y. and Nishio, M., Cryst. Eng. Comm., 2003, 5: 514
42 Nishinari, K., Prog. Colloid Polym. Sci., 2009, 136: 87
43 Paleo, A.J., Silva, J., van Hattum, F.W.J.; Lanceros-Méndez, S. and Ares, A.I., J. Polym. Sci., Part B: Polym. Phys., 2013, 51: 207
44 de Gennes, P.G., "Scaling concepts in polymer physics" Cornell University Press, New York, 1979, p. 105
45 Sahimi, M. and Arbabi, S., Phys. Rev. B, 1993, 47: 703
46 Loiseau, A. and Tassin, J.F., Macromolecules, 2006, 39: 9185
47 Guimont, A., Beyou, E., Martin, G., Sonntag, P. and Cassagnau, P., Macromolecules, 2011, 44: 3893
48 Trappe, V., Prasad, V., Cipelletti, L., Segre, P.N. and Weitz, D.A., Nature, 2001, 411: 772
49 Knauert, S.T., Douglas, J.F. and Starr, F.W., J. Polym. Sci., Part B: Polym. Phys., 2007, 45: 1882
50 Wagner, N.J. and Brady, J.F., Phys. Today, 2009, 62: 27
51 Brown, E., Forman, N.A., Orellana, C.S., Zhang, H.J., Maynor, B.W., Betts, D.E., DeSimone, J.M. and Jaeger, H.M., Nat. Mater., 2010, 9: 220
52 Youssry, M., Madec, L., Soudan, P., Cerbelaud, M., Guyomard, D. and Lestriez, B., Phys. Chem. Chem. Phys., 2013, 15: 14476
53 Yokozeki, T., Schulz, S.C., Buschhorn, S.T. and Schulte, K., Eur. Polym. J., 2012, 48: 1042
54 Yang, J.J., Zhang, Y.Q., Wang, Z.G. and Chen, P., RSC Adv., 2014, 4: 1246
55 Xu, D.H., Wang, Z.G. and Douglas, J.F., Macromolecules, 2008, 41: 815
56 Li, Y., Nie, Y.J., Ma, Y. and Hu, W.B., Chinese J. Polym. Sci., 2013, 31(11): 1590